Urban site characterization using DAS dark fibers on the MIT campus in Cambridge, Massachusetts

Hilary Chang[1] and Nori Nakata[1,2]

Abstract

Telecommunication dark fibers with distributed acoustic sensing (DAS) are a useful survey tool for site characterization in urban environments. In this paper, we introduce our five-day student-led DAS experiment using dark fibers at the Massachusetts Institute of Technology campus in the city of Cambridge. The campus has been identified as an area that is highly susceptible to seismic hazards due to subsurface structure and soil properties. The experiment included survey planning, data acquisition, data analysis, subsurface characterization, and site-response estimations. Rayleigh waves collected by dark fibers in the urban environment are mostly from human activities and contain abundant higher-mode energies. We invert the phase velocity dispersions to resolve the shear-wave velocity (V_S) in the top 120 m of the subsurface. The V_S profiles show low V_S (0.1–0.3 km/s) corresponding to unconsolidated materials such as artificial fills and clays overlying a hard bedrock (1.5–1.8 km/s). The depth to bedrock is 75–95 m on the west campus. The site near the waterfront has a lower V_S and deeper bedrock. The 1D site-response modeling for shear waves suggests that the fundamental resonance frequency is at 0.6 and 1 Hz, with a sediment-to-bedrock amplitude ratio of 6–7. This should be considered in building design to mitigate seismic hazards. Our results agree with previous studies and can bridge the gap between measurements at nearby sites.

Introduction

Site characterization is important for understanding earthquake hazards and promoting seismic-resistant city and building design. In the past, geotechnical properties of the subsurface have been obtained mainly by wells and small seismic surveys at each location. In recent years, the use of seismic array methods for measuring strain and strain rate along dark fibers using distributed acoustic sensing (DAS) has opened another possibility for nonintrusive geophysical survey techniques. Dark fibers are unused backup optic fibers in a telecommunication network. Several studies have demonstrated the use of campus or city dark fibers to characterize velocity structure from the near surface (top 10–150 m) (Ajo-Franklin et al., 2019; Spica et al., 2020; Song et al., 2021; Cheng et al., 2023) to intermediate depth (a few hundreds of meters) (Rodríguez Tribaldos et al., 2021; Shragge et al., 2021). The advantages of using DAS dark fibers for site characterization are that (1) receivers do not need to be deployed and (2) the results are repeatable as long as the cable is still there. However, additional considerations and procedures are required to ensure the data can reach its full potential.

In March 2022, we conducted a dark-fiber experiment using telecommunication cables under the Massachusetts Institute of Technology (MIT) campus. The experiment was supported by the MIT SEG student chapter. Students participated in DAS data collection including renting the equipment, communicating with the interrogator provider (Silixa) and the campus IT team, and planning the logistics of the survey. We collected five days of continuous data with environmental seismic signals and applied the multichannel analysis of surface waves (MASW) (Park et al., 1999) method to characterize the shear-wave velocity structure beneath the campus. In this paper, we describe the experiment including planning, analysis, and interpretation. We also share lessons learned and potential improvements. We envision that new users will find this paper helpful when planning their own dark-fiber experiments.

The MIT campus is located in the city of Cambridge across the Charles River from Boston (Figure 1a). The part of the campus on the north bank of the river has been identified as an area that is susceptible to seismic hazards due to large impedance contrasts and soil properties (Hayles et al., 2001; Brankman and Baise, 2008; Baise et al., 2016). Previous analyses of the shallow structure in this area (within 1 km from the main campus) used boring data (BSCE, 1961; Mabee et al., 2023a), passive seismic methods (Kummer, 1998; Hayles et al., 2001; Yilar et al., 2017; Mabee et al., 2023a), and active seismic surveys (Santagata and Kang, 2007; Thompson et al., 2014). The boring method is costly and intrusive. The seismic surveys require the deployment of seismometers and, for an active survey, seismic sources. In this study, we apply the MASW method to the strain rate measured from the dark fibers on the MIT campus. The MASW method uses the dispersion of surface waves to characterize the shear-wave velocity structure. The dark fibers connecting the buildings can be used as seismic sensors that have already been deployed in place. Hence, the survey minimizes disturbances to the area.

In the following, we first provide a brief introduction to the near-surface geology of the study area. Next, we outline how we prepared for the survey (e.g., selecting the cable, choosing survey parameters, and locating the channels). We demonstrate that for horizontal-laying cables, simple friction coupling is sufficient to record environmental signals for ambient noise studies. Then, we present data analysis procedures for extracting surface waves from five days of ambient noise, inverting for the subsurface structure,

---

[1]Massachusetts Institute of Technology, Department of Earth, Atmospheric, and Planetary Sciences, Cambridge, Massachusetts, USA. E-mail: hilarych@mit.edu; nnakata@mit.edu.
[2]Lawrence Berkeley National Laboratory, Berkeley, California, USA.

a Approximate route and tap test locations
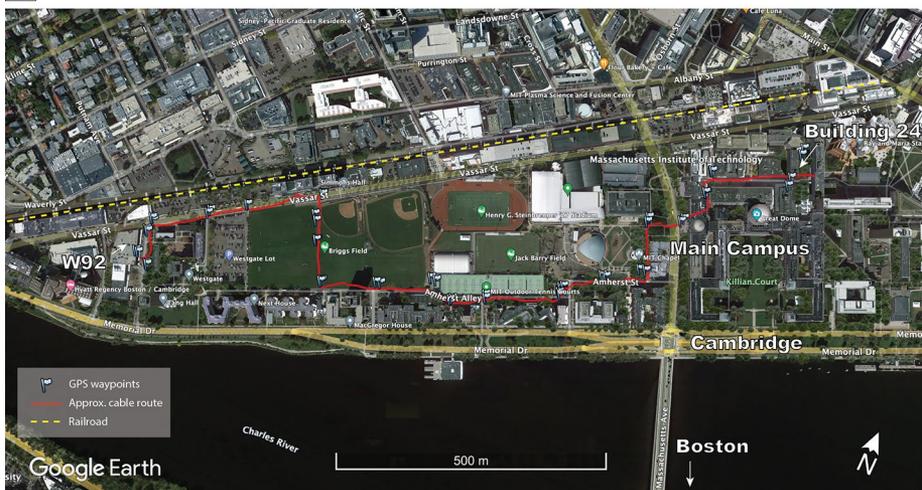
b Interpolated route between tap test locations
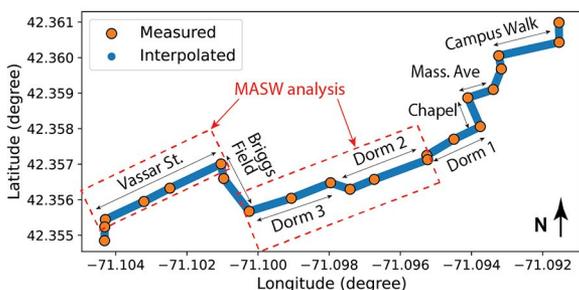
Figure 1. Aerial view of the study area and telecommunication cable. We focus on the main campus, which is situated between the Charles River and a railroad (marked by the yellow dashed line). The cable begins in building 24 to the east and ends at building W92 to the west, with the majority of it lying in the west campus (west of Massachusetts Avenue). We conduct tap tests (indicated by flags in [a] and orange dots in [b]) and linearly interpolate between tapped locations to locate individual channels on the cable (shown in blue in [b]). The red dashed boxes indicate the two cable sections where we perform MASW. The map in (a) is modified from Google Earth map data as of March 2022.

Geologic Units	Thickness
Landfills	(3 - 9 m)
Organics	(1.5 - 9 m)
Outwash Deposits	(0 - 7.5 m)
Marine Clay (Boston Blue Clay) (Stiff) (Medium) (Soft)	(12 - 43 m)
Outwash Deposits	(0 - 3 m)
Glacial Till	(1.5 - 9 m)
Bedrock (Cambridge Argillite)	

10 - 80 m

Figure 2. Near-surface geologic units for the study area (modified from Johnson, 1989). The range of thickness includes areas on the waterfronts and many low-lying regions in the Greater Boston area. The depth to bedrock ranges from 10 to 80 m (Baise et al., 2016).

and estimating site amplifications. Our results agree with general expectations for this region and can bridge the gap between nearby measurements from previous studies.

Near-surface geology

In the Greater Boston area, the surficial geology in many low-lying regions and waterfronts is classified as artificial landfill, which includes a mix of sands, silts, and gravels. These landfills were made during rapid urbanization from the 19th to early 20th century (Johnson, 1989; Woodhouse et al., 1991). Before the 1975 enactment of seismic-resistant building designs, many buildings were built on these unengineered (without meeting today's standards on seismic loading) loose fills, including areas on the MIT campus. Other unconsolidated materials exist under the landfills such as organics, outwash deposits (sands and gravels), marine clays, and glacial tills (Figure 2) (Johnson, 1989), with a thickness that ranges from 10 to 80 m, lying on hard bedrock. The subsurface condition makes these areas highly susceptible to seismic hazards. The chance of exposure to strong motion is not high (USGS Earthquake Hazards Program, 2024) because New England is not located along an active tectonic plate margin. However, destructive earthquakes have still occurred (e.g., 1727 and 1755 with a Modified Mercalli Intensity of 7 and 8, respectively) (Woodhouse et al., 1991). A large portion of the flat region in Boston and Cambridge near the Charles River is class E in the National Earthquake Hazards Reduction Program (Mabee et al., 2023b), corresponding to soft clay with a very low shear-wave velocity (less than 180 m/s) in the top 30 m. The strong impedance contrast and soil contents tend to amplify ground motion, with a high risk of soil liquefaction (Brankman and Baise, 2008; Baise et al., 2016). Previous studies found that the ground motions are highly variable in the Boston area, likely due to variabilities in subsurface layer thickness (Kummer, 1998; Ebel and Hart, 2001; Hayles et al., 2001).

Preparations and the survey

Identifying the cable. Several cable routes are available across the campus. With assistance from MIT Information Systems and Technology, we identified one route that passes through the middle of the campus (red route in Figure 1a). The route includes the following locations: a sidewalk along the street (Vassar Street), a sports field (Briggs Field), student residences (dorms 1–3), MIT Chapel, a crosswalk in front of the main
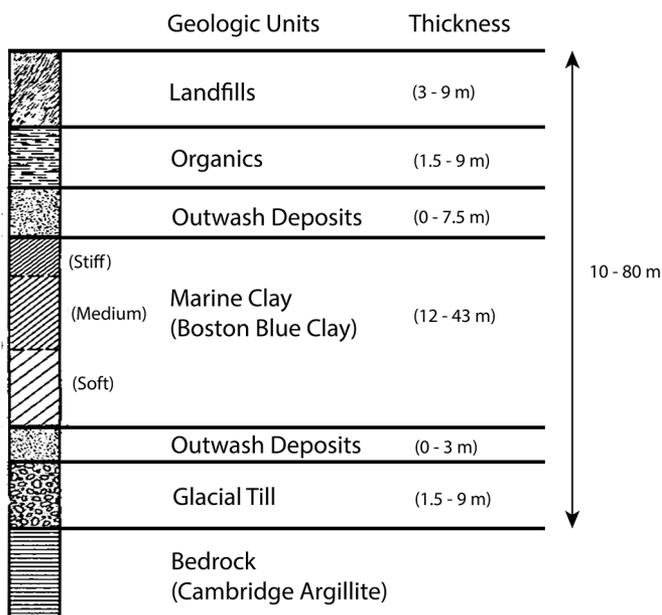
entrance (Massachusetts Avenue), and a pathway on campus (Campus Walk). The cable starts from building 24 on the east and continues to building W92 on the west, with a total length of 2 km. A railroad runs on the north side of the campus. The railroad is used for internal equipment transferring for the public transportation system, which has little traffic and mostly operates overnight.

The dark fibers in the selected cable are single mode. The fibers are continuous with fusion splicing, allowing small optical signal losses from end to end. Cables connected via physical connectors would suffer from high optical losses and would not be ideal. Along the route, the cables are protected in layers of PVC and plastic tubes (Figure 3a). The tubes lie horizontally within the foamed metal conduits, which are filled with air. The coupling relies simply on gravity and friction. In our experiment, the portion inside the buildings is not usable because the tubes are hanging from the ceiling with no coupling to the ground. Outside the buildings, the tubes are buried 2–5 ft below the surface and can be tracked by manholes.

Setting the DAS system. We use the Silixa iDAS 2.0 interrogator. We also use a gauge length of 10 m, a sampling interval of 1 m, and an output sampling frequency of 1000 Hz. Setting parameters of the interrogator depend on the type of interrogator, length of cable, and desired resolution. According to the iDAS instructions provided by Silixa, nonideal settings mostly do not affect signals but can decrease signal-to-noise ratio (S/N) due to instrument-related noise. For ambient-noise applications, high instrumental noise can affect the ability to extract coherent waves from environmental noise. A longer cable length reduces S/N due to a reduced maximum pulsing frequency (only one pulse can travel in the fibers at a time for iDAS). Although a longer gauge length improves S/N, it limits the minimum wavelength we can resolve (twice the gauge length) and limits the shallowest depth we can probe for surface-wave applications.

The optical power also needs to be properly adjusted so the amplitude of the light decreases linearly with increasing distance from the light source at the interrogator.

We connect the interrogator to the cable at building 24 (Figures 3b and 3c). At MIT, the server room that hosts the connectors has access restrictions, and the experiment needs to be approved by the management team. This server room is above ground level, allowing good signals for the GPS antenna to measure accurate time stamps during data collection. Although the interrogator has an internal feedback system to counter small movements, it is still important to place the interrogator on a stable platform because vibrations at the interrogator can destroy the phase-shift measurements of the entire cable (causing in-phase noise across all channels). We recommend substituting the table in Figure 3b with a more stable platform.

Locating the channels. We perform a tap test to locate the channels along the cable. During the tap test, we take GPS measurements along the identified route while hammering to create a signal pattern (Figure 4). Manholes are a good tracker for cable locations, and they generate clear tap signals via a hammer. Later, we identify the signal pattern in the data and associate the GPS coordinates with the channels that recorded the blows. We recommend conducting the tap test during a quiet time (e.g., 2:00–3:00 a.m.) because distinguishing the tap signals from many other environmental noises can be difficult during the day. We conduct tap tests at kinks along the route and linearly interpolate the channel locations between the kinks (Figure 1b).

Data analysis

Preprocessing of the raw data. After five days of continuous recording, we obtained 1.8 TB of data with 2050 channels and a sampling rate of 1000 Hz. The data are stored in 16-bit integers to save space. The unit of the raw data is the phase-shift rate (radian per time sample over a gauge length). We convert the data

Cables are inside the PVC tubes

Monitor

iDAS Interrogator

E2000/APC Connector
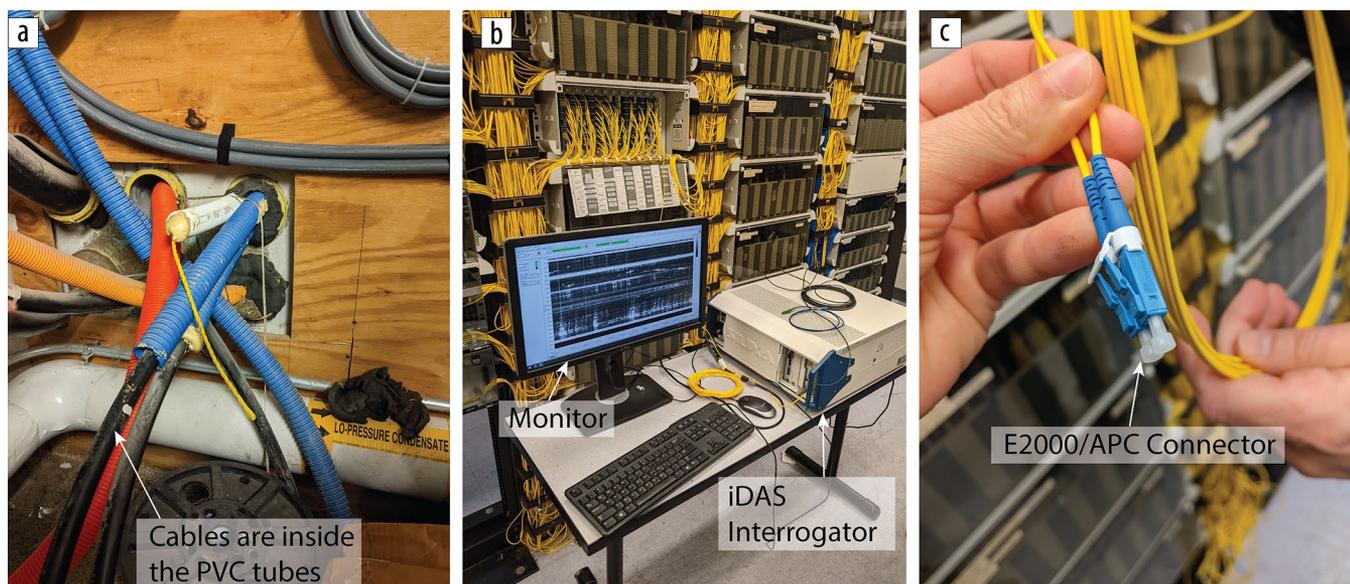
Figure 3. Pictures of the cables and the experiment setup. (a) The burial condition of the cables. The cables are inside air-filled conduits and can be exposed where they enter the building. (b) and (c) The interrogator is connected to the cable in the server room in building 24. Note that we recommend replacing the table supporting the interrogator with a more stable platform to prevent interrogator-generated noise.

Special Section: Optical fiber
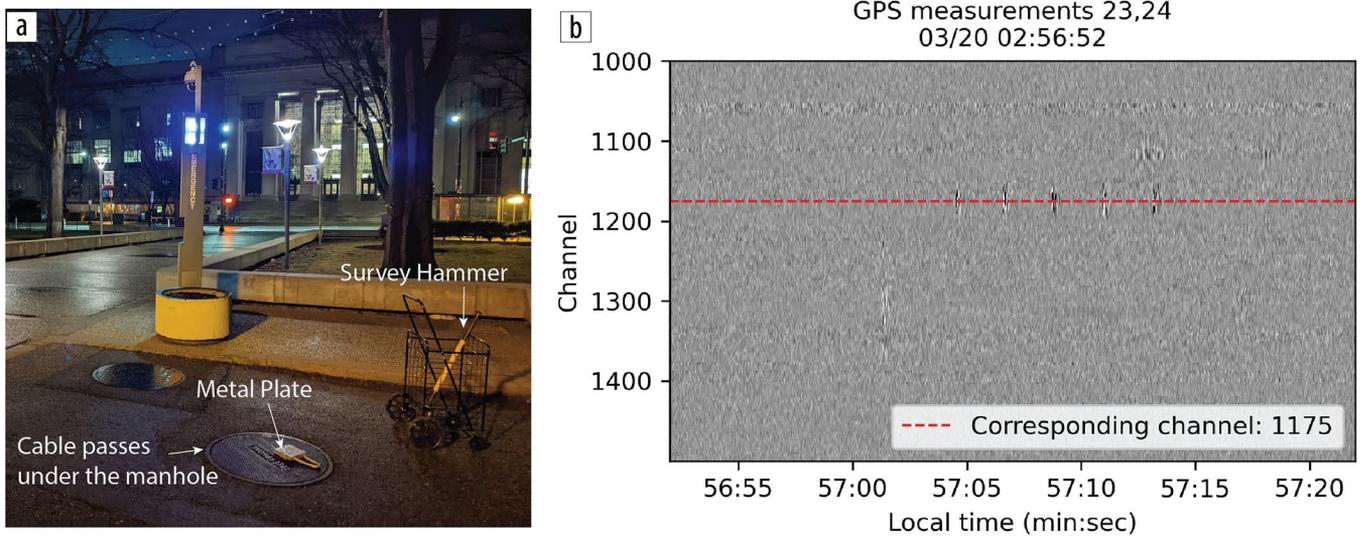
Figure 4. Tap test for locating the channels on the telecommunication cable. In (a), we hammered on the metal plate placed on manholes along the cable route to create a recognizable signal pattern while taking GPS measurements (we take the average coordinate of two GPS measurements at a point). We later identify the signal pattern in the data (five blows shown in [b]) by the GPS times and link the coordinates to the corresponding channels.
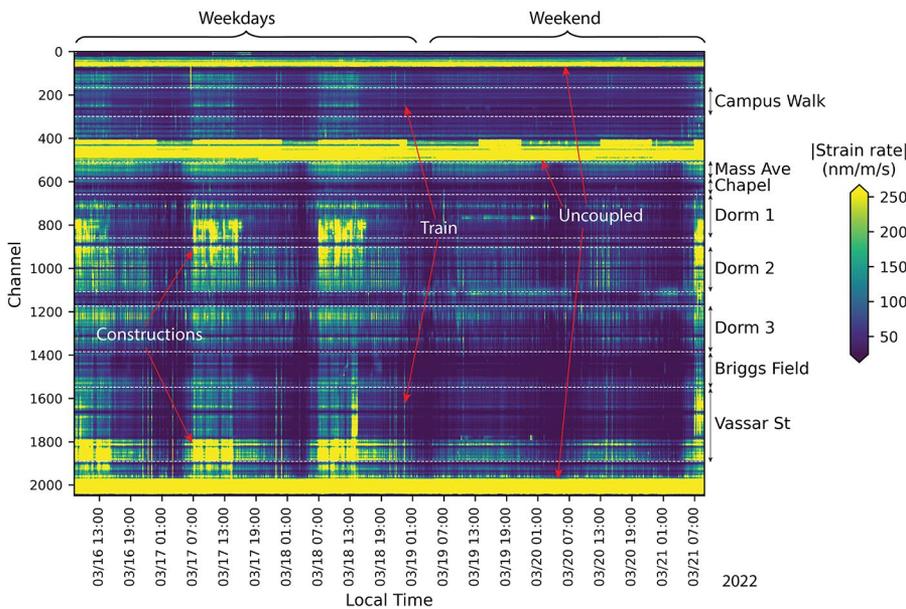
Figure 5. Root-mean-square amplitudes calculated in a sliding 10-minute time window with a hop length of 5 minutes. The uncoupled portions are located inside buildings where the cables hang on the ceiling without ground coupling.

related to filtering in the frequency domain, is important to prevent artifacts in later processing. For ambient noise processing where we need to frequently extract time windows at different channels from a large data set, it is convenient to store data using Hierarchical Data Format 5 (HDF5) (White et al., 2023). We combine the original 30 s files into one data block in an HDF5 file. Then, for each five-day trace, we de-mean, detrend, taper both ends, apply an anti-aliasing low-pass filter, and downsample the trace to a sampling frequency of 200 Hz. In cases where large spikes are present, an initial quality control to clip large-amplitude spikes may be required.

Environmental signals

Time and space variations of the DAS strain rate show that the most intense energy sources are human activities. The strain rate amplitudes are highest during the daytime on weekdays (Figure 5). The construction of new buildings in front of dorm 1 and at the end of Vassar Street generates intense signals during work hours. The signals of slow-passing trains along the north side of the campus are visible where the cable is close to the railway (Campus Walk and Vassar Street). Indoor portions of the cable always have large amplitudes (horizontal stripes), likely due to resonances in uncoupled conditions.

Figure 6 shows the zoomed-in view of these environmental signals. The cable on Vassar Street is aligned with the street, and the slope of the signal corresponds to the velocity of passing vehicles/trains/bikes. Signals with speeds of about 18 m/s (65 km/hour) going in both directions are fast-traveling cars. The

to strain or strain rate to determine the actual elongation that the fibers experienced. The unit does not affect the results of ambient noise interferometry. The conversion involves multiplying the data by a factor given by the interrogator provider. We convert the data to a unit of nm/m/s using a factor of $116 \times 2^{-13} \times 1000$ Hz/10 m, where 116 corresponds to conversion from 1 radian of phase shift to 1 nm of elongation over a gauge length, 2^{-13} is related to float-to-integer scaling (for data compression), 1000 Hz is the sampling frequency, and 10 m is the gauge length. Different interrogators would have different conversion factors.

The data often have spikes and drifts due to noise from the interrogator and the environment (e.g., temperature). Hence, proper data treatment before processing, especially anything

signal traveling with a constant speed of 1.4 m/s (5 km/hour) is likely a bike. The high-energy packet with a velocity of 5 m/s (18 km/hour) corresponds to a small train (two carts) passing at a slow speed (spotted by the author). The construction causes large-amplitude waves (a few microstrains per second) (Figure 6b) with an apparent speed of 0.5 km/s, which is the higher bound of the actual wave speed because the incident angle may not be zero with the direction of the cable. Human activities from traffic, pedestrians, and construction during the rush hour are most intense between 2 and 30 Hz (Figure 7). Resonance of uncoupled cables generates high-frequency noise (10–60 Hz). Later in the ambient noise analysis, we suppress large-amplitude transient noise by applying quality controls (explained next) before extracting surface waves (bottom row in Figure 7).

Ambient noise surface waves

We calculate cross coherence between channel pairs along the cable. The cross coherence in the frequency domain ($cc(f)$) is defined as

$$ cc\left(f\right) = \frac{u(f)\,u_0^*(f)}{|u(f)||u_0(f)|}, \qquad (1) $$

where $u(f)$ and $u_0(f)$ are the strain rate spectra at the receiver and the virtual source channels, respectively (Aki, 1957; Nakata et al., 2011). The asterisk indicates complex conjugation. The cross coherence discards the amplitude information by normalizing the input data by their spectral amplitudes. Hence, it is more stable than other interferometry methods, such as deconvolution, when noise with large and varying amplitude exists (Nakata et al., 2011). We use a one-minute time window and step with a 90% overlap in time. Preprocessing before calculating the cross coherence includes de-meaning, detrending, tapering both ends, time-domain normalization (using a 10 s running absolute mean), and frequency normalization (spectral whitening), similar to the procedures in Bensen et al. (2007). It also includes bandpass filtering the data between 0.1 and 99 Hz. We add white noise that is 0.1% of the average spectral amplitude in the denominator of equation 1 for stability (Nakata et al., 2013).

We perform a quality control to further minimize the influence of large transient noise. We discard strain rate data when the envelope exceeds an amplitude threshold. That is, we require
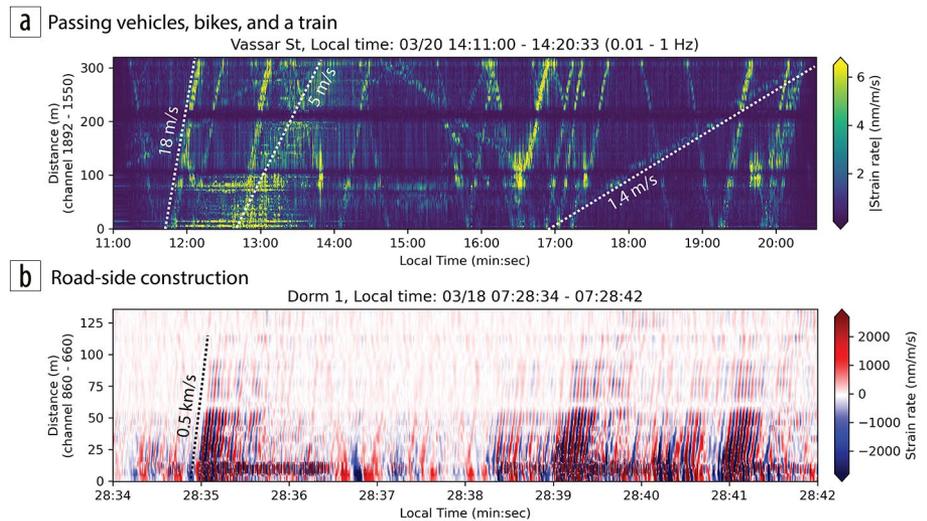
Figure 6. Signals from human activities: (a) passing vehicles along Vassar Street and (b) construction in front of dorm 1. The smearing signal (5 m/s) in (a) corresponds to a small train with a slow speed. The construction produces large-amplitude waves (micrometer-scale strain rate) in (b).
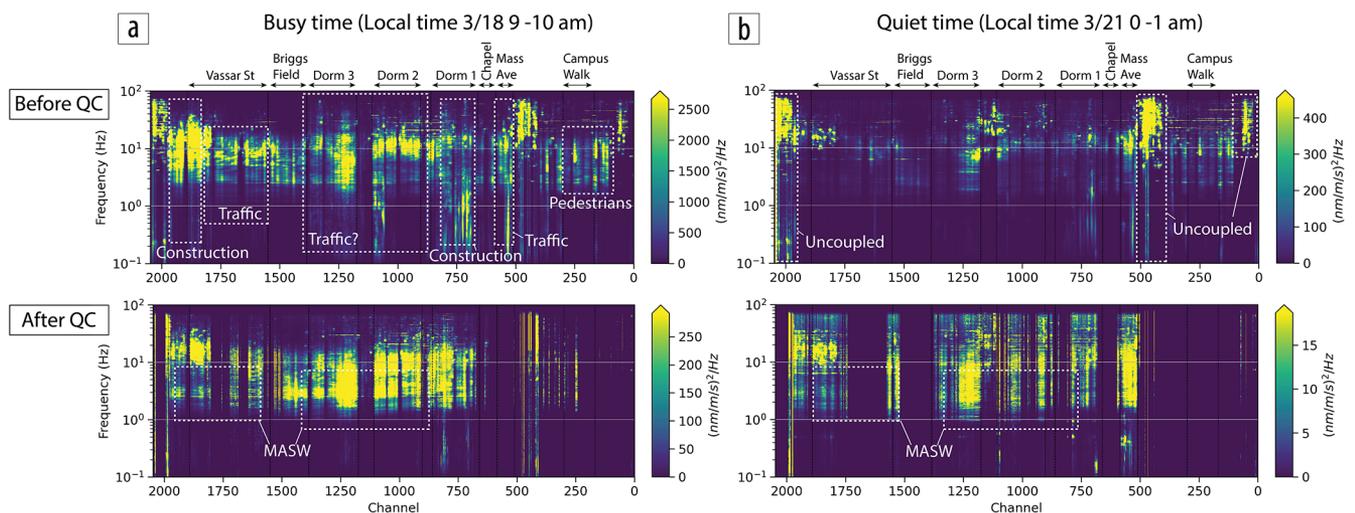
Figure 7. Power-spectral density (PSD) of strain rates along the cable at (a) a busy hour and (b) a quiet hour. The PSD is calculated using a 1-minute time window and is averaged over 1 hour. The top row shows the original data, and the bottom row shows data after quality control, in which we discard windows where the amplitude exceeds a threshold defined by the standard deviation (equation 2). The white dashed boxes in the top row denote identified environmental noises. Those in the bottom row highlight the cable sections and frequency range where we successfully extract coherent surface waves and apply MASW. The color bars are trimmed at the 95 percentile.
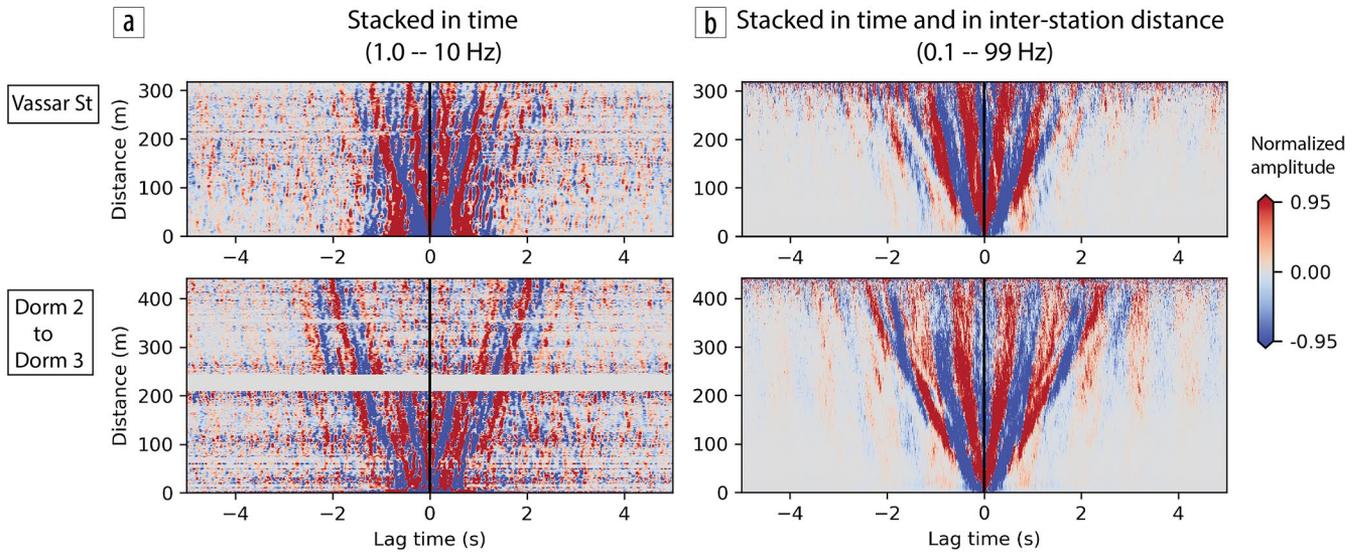
Figure 8. Coherograms (a) stacked in time and (b) stacked in time and interstation distance (i.e., common virtual shot gather). The top row shows coherograms along Vassar Street, and the bottom row shows those from dorms 2 and 3. The coherograms in (a) use a virtual source on the west end of these sections. The bandpass filter in (a) (1.0–10 Hz) is only for visualization purposes. The bandpass filter in (b) (0.1–99 Hz) is applied to the stacked coherogram before proceeding with the dispersion analysis.

$$max\left(A_{1min}\right) \; < \; \overline{A_{1hr}} + 2\sigma_{A_{1hr}}, \qquad (2)$$

where A_{1min} is the envelope of the 1-minute time window. $\overline{A_{1hr}}$ and $\sigma_{A_{1hr}}$ are the median envelope and its standard deviation over 1 hour, respectively. The factor of 2 was determined after repeated testing, during which we tried to reject noisy data while keeping as many windows as possible for stacking. The quality control rejects more than 96% of the windows for most channels. We stack the remaining time windows (about 6000 windows on average and 35,000 windows at the most) for each channel pair. We use phase-weighted stacking (Schimmel and Paulssen, 1997), which significantly improves the S/N (also recommended by Dou et al. [2017] and Rodríguez Tribaldos et al. [2021]).

We select two inline sections that show clear Rayleigh waves: one along Vassar Street (310 m in total) and one from dorms 2 to 3 (440 m in total). Figure 8 shows the coherograms along the two selected sections. We stack the coherograms with the same inter-channel distances (±1 m) using phase-weighted stacking and bandpass filter the stacked coherogram between 0.1 and 99 Hz. Because the DAS measurement is only sensitive to particle motion along the fiber direction, the waves in the coherograms of inline sections are dominantly Rayleigh waves (Martin et al., 2021). The Rayleigh waves start from the origin and exhibit good symmetry between positive and negative lag times (Figure 8a). Asymmetry in the cross-coherence wavefields may be attributed to unevenly distributed noise sources (Stehly et al., 2006) or different coupling conditions of the cable (Zeng et al., 2017). The former cause may bias the phase velocity measurements (Yao and Van Der Hilst, 2009; Harmon et al., 2010) if the sources are out of line with the receiver pairs (e.g., Figure 16 in Lin et al. [2008]). The good symmetry in Figure 8a suggests that the phase velocity is not likely biased by unevenly distributed sources.

Figure 9a shows the phase velocity dispersion of the Rayleigh waves. The Rayleigh waves contain strong higher-mode energy. The highest usable frequency is limited by the gauge length, as

waves with wavelengths shorter than twice the gauge length are spatially aliased (area to the right of the solid black curve). The lower-frequency bound is determined by the length of the cable section (black dashed curve). Beyond these boundaries, the S/N is low, and picking the dispersion curve is difficult.

Shear-wave velocity inversion

To apply the MASW method, we manually pick the dispersion curves by using the MATLAB package MASW Dispersion Curve (Schuh, 2024). Then, we invert the dispersion curves for the shear-wave velocity structure at Vassar Street and dorms 2 and 3 (Figure 9b). The inversion is done by evodcinv (Luu, 2021), which is a Python library that uses an evolution algorithm to find the best set of layer thickness and velocity, given a rough initial bound of each layer. We start the inversion using a reference model based on the average landfill site profile in Baise et al. (2016). We find that the fundamental mode is weak at Vassar Street and likely missing at dorms 2 and 3. Otherwise, we cannot generate a proper fit to the picks (small plus signs and red dashed curves in Figure 9a).

The V_S profiles show that both locations have velocities as low as 100–300 m/s at the near surface (Figure 9b). The large velocity contrasts at 75 m under Vassar Street and about 90 m under dorms 2 and 3 are likely the interface between the soil and the bedrock. The velocity reversal between 20 and 55 m at dorms 2 and 3 is likely related to Boston Blue Clay, which consists of a stiffer upper layer and a soft bottom layer (Figure 2) (Johnson, 1989; Santagata and Kang, 2007; Thompson et al., 2014).

In Figure 10, we compare the results with those of previous surveys at nearby sites (labeled in numbers). The bedrock depth is within the range (50–100 m) of previous surveys. Our results support previous measurements that indicate a low V_S soil column and lower bedrock depth (90 m plus) near the riverfront from Boston University Bridge to Harvard Bridge (measurements from Hayles et al. [2001] and Yilar et al. [2017] in the dashed box in Figure 10). The velocity reversal associated with the Boston Blue

Clay was also observed at Tang Hall by Hayles et al. (2001) and at the Stata Center of MIT by Santagata and Kang (2007) (3 and 4 in Figure 10).

Site amplification simulation

We simulate ground motion transfer functions at Vassar Street and dorms 2 and 3 using the shear-wave velocity profile. The simulation is implemented by Nrattle (Boore, 2005), which calculates a full-resonance solution for amplifications of horizontally polarized shear waves due to impedance contrasts in the structure. We assume a linear site response, which is suitable for modeling a region with moderate seismicity such as Boston (Baise et al., 2016). The amplification is relative to the ground motion of a homogeneous structure (i.e., soil-to-rock amplitude ratio). We use the following parameters based on a local soil model in Boston (Table 1 in Baise et al. [2016]): quality factor (Q) = 20, density (ρ) = 1.65 g/cm^3 for the top 100 m, and ρ = 2.75 g/cm^3 and V_S = 1.8 km/s for below 100 m. We calculate the transfer function for shear waves with a vertical-incidence angle from a source in the half-space.

Figure 11 shows the ground motion transfer functions along Vassar Street and dorms 2 and 3. Vassar Street has resonance peaks at 1 and 2.5 Hz, while dorms 2 and 3 have a lower-frequency peak at 0.6 Hz due to a deeper depth to bedrock and a lower velocity in the soil column. Both sites have a maximum amplification of 6–7 times relative to bedrock. The results agree with measurements in Hayles et al. (2001) at Tang Hall (3 in Figure 10a). They estimated a resonance frequency between 0.67 and 1.0 Hz and a soil-to-rock amplitude ratio of 7.6 based on microtremor H/V measurements and a 1D simulation using V_S from nearby well-log data (cyan circles in Figure 10b).

Discussion

The consistency between our results and previous studies and geologic records demonstrates the feasibility of using dark fibers for site characterization. The clear Rayleigh waves from the western part
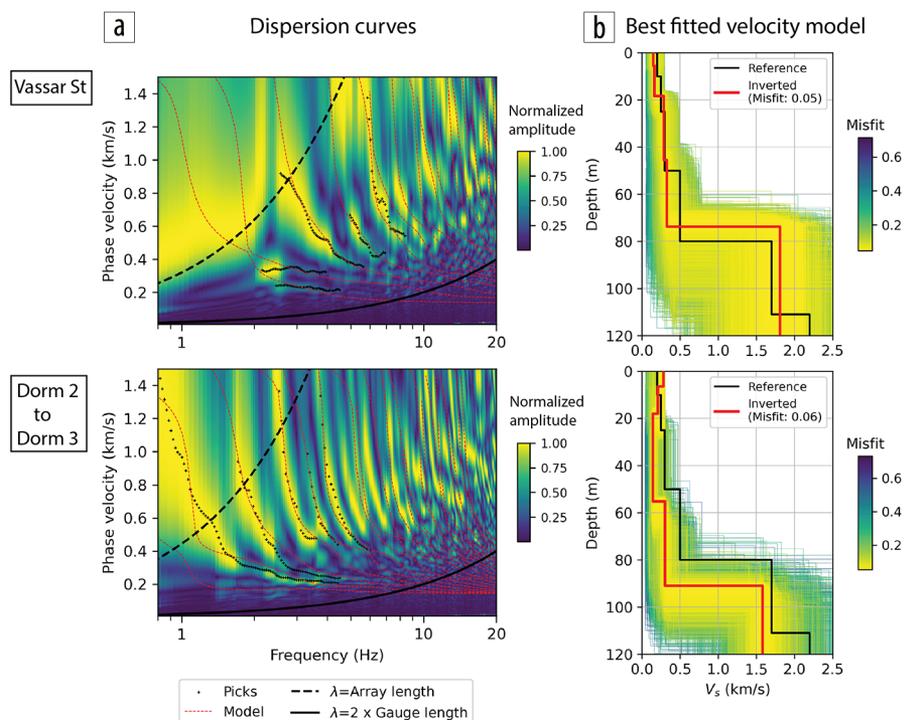
Figure 9. (a) Phase-velocity dispersions and (b) inverted shear-wave velocity structure at Vassar Street (top) and dorms 2 and 3 (bottom). In (a), plus symbols are manual picks, and the red dashed curves are the best-fitted dispersions after the inversion. The dashed and solid black curves correspond to wavelengths (λ) equal to the maximum channel distances along the section and to 2 times the gauge length, respectively. In (b), the red and black profiles are the inverted model and the reference model from Baise et al. (2016), respectively. The colored profiles are evolutions during the inversion (Luu, 2021).
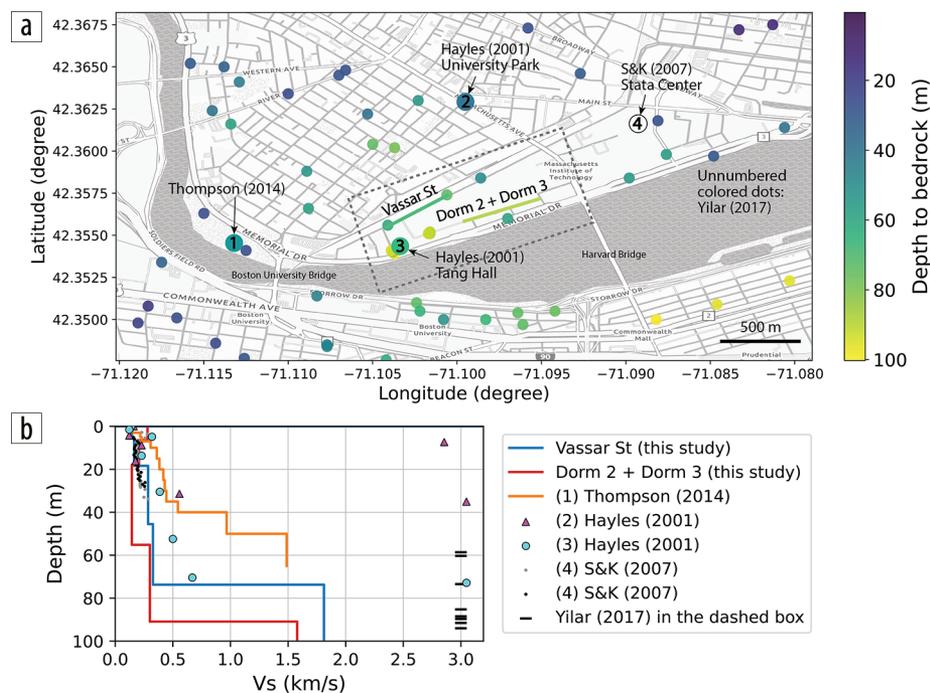
Figure 10. Comparison of the (a) bedrock depth and (b) V_S structure in this study with previous studies. Our results at Vassar Street and dorm 2 are the colored lines in (a) inside the dashed box. Unnumbered colored circles are bedrock depth results from Yilar et al. (2017). Numbered circles are results from (1) Thompson et al. (2014), (2) and (3) Hayles et al. (2001), and (4) Santagata and Kang (2007) (which did not have bedrock depth but only V_S profile). The V_S profiles in these studies are shown in (b). The dashed box encloses sites less than 250 m from the cables.

of the campus (Figure 8) show that the frictional coupling of horizontal-lying cables is sufficient for recording ambient noise surface waves. However, the missing modes (Figure 9a) could potentially result in mode misidentification and cause erroneous V_S inversion. We speculate that the missing mode is caused by the noise source excitation (Aki and Richards, 2002) and/or site-specific attenuation, but we need more data to confirm this. On the other hand, cable sections on the east campus (east of MIT Chapel) do not have much available ambient noise that meets the quality-control criteria. At the chapel and across Massachusetts Avenue, the inline cables are too short (less than 100 m), which limits their ability to measure the phase velocity below 10 Hz (while that is the dominant frequency band of the surface wave in the environment). Along Campus Walk, the S/N is low due to less activity and weak anthropogenic noise (Figure 7). A longer data-collection period can enhance the S/N of coherent surface waves (Ritzwoller and Feng, 2019).

A nonuniformly distributed noise source can bias phase velocity measurements of ambient noise surface waves (Yao and Van Der Hilst, 2009). In this experiment, as generally expected in an urban area, the noise sources are dominantly cultural noises (Figures 5 and 6), which are most likely nonuniform. The coherograms still exhibit good symmetry without symptoms of noise source anisotropy as we perform careful quality control to discard strong local transient noise in the data. The directivity of DAS also acts as a filter that enhances Rayleigh waves propagating along the cable (Bakku, 2015; Martin et al., 2021), which produces no phase biases, even when the energy source is stronger in one direction (Figure 16 in Lin et al., 2008). Another uncertainty of using dark fibers comes from channel location. In this experiment, the ability to track the cable by manholes, which can generate large signals with a single hammer, allows us to precisely locate the channels during the tap test and minimize location errors.

To improve the experiment, having a collocated vertical-component geophone or seismometer that records continuous data concurrently with DAS would add possibilities to many other applications. First, a vertical-component instrument can help us separate different types of waves (e.g., Rayleigh and Love waves). While a horizontal-component sensor can capture both Rayleigh and Love waves, the vertical-component sensor is dominated by Rayleigh waves but not Love waves. This would allow a more precise V_S inversion using multiple types of waves. Second, we can apply the horizontal-to-vertical spectral ratio (H/V) method and verify the depth of the interface with amplitude information (e.g., Spica et al., 2020). Third, a vertical-component instrument is useful for distinguishing teleseismic arrivals that can potentially be used in receiver functions analysis to explore deeper structures (e.g., Yu et al., 2019).
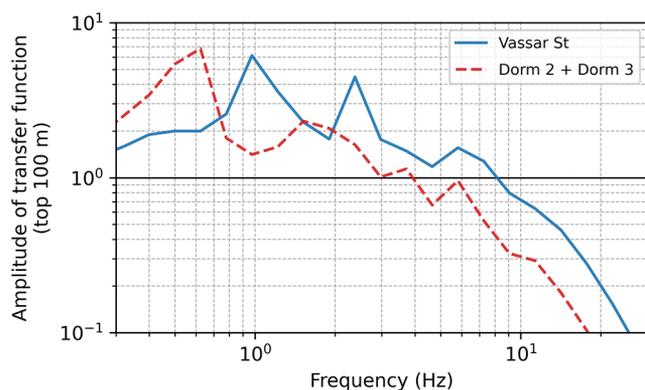
Conclusion

The use of dark fibers with DAS provides a nonintrusive tool for site characterization in the urban environment. In this study, we use five days of ambient noise recorded by the dark fibers on the MIT campus to characterize the near-surface structure. The dark fibers can record abundant environmental signals with a simple frictional coupling in horizontally laid air-filled conduits. We observe abundant higher modes but find weak fundamental-mode Rayleigh waves in the data.

We resolve 1D shear-wave velocity profiles on the top 120 m at Vassar Street and in front of the student residences (dorms 2 and 3) on the west campus. The fundamental frequency of ground motion for vertically-incident shear waves is 0.6 Hz along Vassar Street and 1.0 Hz at the two dorms, with an amplification of 6–7 times relative to that of the bedrock. The results agree with previous studies at nearby sites. The agreement supports the use of dark fibers for site characterization in populated regions and potentially for time-lapse monitoring of changes in soil properties (e.g., before and after flooding).

A DAS survey using dark fibers does not require deploying additional receivers. Using an interrogator to obtain measurements is also straightforward. However, there are considerations including selecting routes, getting access, calibrating the survey, and checking data quality. These considerations can pose barriers in an experiment, and poor decisions may affect the usability and potential of the collected data. There are also limitations due to the nature of the measurements (e.g., the high-frequency resolution limited by gauge length in Figure 9a). In this paper, we present the procedures for others to undertake such experiments, as dark fibers can provide useful information for mitigating seismic hazards in many urban areas. **TLE**

Figure 11. Transfer functions of vertically incident and horizontally polarized S waves based on the shear-wave velocity profiles in the top 100 m. The values are relative to a homogeneous structure in the top 100 m. An amplitude of 1 (horizontal black line) means no amplification.

chapter members Aarti Dwivedi, Sarah Greer, and Ekaterina Bolotskaya for providing feedback on the experiment plan. We appreciate the comments from an anonymous reviewer who helped improve the manuscript.

Data and materials availability

Data associated with this research are available, and upon request, can be obtained by contacting the corresponding author.

Corresponding author: hilarych@mit.edu

References

Ajo-Franklin, J. B., S. Dou, N. J. Lindsey, I. Monga, C. Tracy, M. Robertson, V. Rodriguez Tribaldos et al., 2019, Distributed acoustic sensing using dark fiber for near-surface characterization and broad-band seismic event detection: Scientific Reports, **9**, https://doi.org/10.1038/s41598-018-36675-8.

Aki, K., 1957, Space and time spectra of stationary stochastic waves, with special reference to microtremors: Bulletin of the Earthquake Research Institute, **35**, 415–456.

Aki, K., and P. G. Richards, 2002, Quantitative seismology, second edition: University Science Books.

Baise, L. G., J. Kaklamanos, B. M. Berry, and E. M. Thompson, 2016, Soil amplification with a strong impedance contrast: Boston, Massachusetts: Engineering Geology, **202**, 1–13, https://doi.org/10.1016/j.enggeo.2015.12.016.

Bakku, S. K., 2015, Fracture characterization from seismic measurements in a borehole: PhD thesis, Massachusetts Institute of Technology.

Bensen, G. D., M. H. Ritzwoller, M. P. Barmin, A. L. Levshin, F. Lin, M. P. Moschetti, N. M. Shapiro, and Y. Yang, 2007, Processing seismic ambient noise data to obtain reliable broad-band surface wave dispersion measurements: Geophysical Journal International, **169**, no. 3, 1239–1260, https://doi.org/10.1111/j.1365-246X.2007.03374.x.

Boore, D. M., 2005, SMSIM — Fortran programs for simulating ground motions from earthquakes: Version 2.3 — A revision of OFR 96–80–A: U.S. Geological Survey.

Brankman, C. M., and L. G. Baise, 2008, Liquefaction susceptibility mapping in Boston, Massachusetts: Environmental and Engineering Geoscience, **14**, no. 1, 1–16, https://doi.org/10.2113/gseegeosci.14.1.1.

BSCE, 1961, Boring data from Greater Boston: Boston Society of Civil Engineers.

Cheng, F., J. B. Ajo-Franklin, and V. Rodriguez Tribaldos, 2023, High-resolution near-surface imaging at the basin scale using dark fiber and distributed acoustic sensing: Toward site effect estimation in urban environments: Journal of Geophysical Research: Solid Earth, **128**, no. 9, https://doi.org/10.1029/2023JB026957.

Dou, S., N. Lindsey, A. M. Wagner, T. M. Daley, B. Freifeld, M. Robertson, J. Peterson, C. Ulrich, E. R. Martin, and J. B. Ajo-Franklin, 2017, Distributed acoustic sensing for seismic monitoring of the near surface: A traffic-noise interferometry case study: Scientific Reports, **7**, no. 1, https://doi.org/10.1038/s41598-017-11986-4.

Ebel, J. E., and K. A. Hart, 2001, Observational evidence for amplification of earthquake ground motions in Boston and vicinity: Civil Engineering Practice, **16**, 5–16.

Harmon, N., C. Rychert, and P. Gerstoft, 2010, Distribution of noise sources for seismic interferometry: Geophysical Journal International, **183**, no. 3, 1470–1484, https://doi.org/10.1111/j.1365-246X.2010.04802.x.

Hayles, K. E., J. E. Ebel, and A. Urzua, 2001, Microtremor measurements to obtain resonant frequencies and ground shaking amplification for soil sites in Boston: Civil Engineering Practice, **16**, no. 2, 17–36.

Johnson, E. G., 1989, Geotechnical characteristics of the Boston area: Civil Engineering Practice, **4**, no. 1, 53–64.

Kummer, K. E., 1998, Microtremor measurements to obtain resonant frequencies and ground shaking amplification for soil sites in Boston, Massachusetts: Boston College.

Lin, F.-C., M. P. Moschetti, and M. H. Ritzwoller, 2008, Surface wave tomography of the western United States from ambient seismic noise: Rayleigh and Love wave phase velocity maps: Geophysical Journal International, **173**, no. 1, 281–298, https://doi.org/10.1111/j.1365-246X.2008.03720.x.

Luu, K., 2021, evodcinv: Inversion of dispersion curves using Evolutionary Algorithms: Zenodo, https://doi.org/10.5281/zenodo.10112876.

Mabee, S. B., C. C. Duncan, B. Clement, and M. A. Pontrelli, 2023a, Massachusetts Depth to Bedrock Project: Massachusetts Department of Transportation, Research Report.

Mabee, S. B., M. A. Pontrelli, C. C. Duncan, and W. P. Clement, 2023b, NEHRP soil classification map of Massachusetts: Massachusetts Geological Survey Miscellaneous Map 23-01, 1:125,000 scale.

Martin, E. R., N. J. Lindsey, J. B. Ajo-Franklin, and B. L. Biondi, 2021, Introduction to interferometry of fiber-optic strain measurements, *in* Y. Li, M. Karrenbach, and J. B. Ajo-Franklin, eds., Distributed acoustic sensing in geophysics: Methods and applications: American Geophysical Union, 111–129, https://doi.org/10.1002/9781119521808.ch9.

Nakata, N., R. Snieder, S. Kuroda, S. Ito, T. Aizawa, and T. Kunimi, 2013, Monitoring a building using deconvolution interferometry: I: Earthquake-data analysis: Bulletin of the Seismological Society of America, **103**, no. 3, 1662–1678, https://doi.org/10.1785/0120120291.

Nakata, N., R. Snieder, T. Tsuji, K. Larner, and T. Matsuoka, 2011, Shear wave imaging from traffic noise using seismic interferometry by cross-coherence: Geophysics, **76**, no. 6, SA97–SA106, https://doi.org/10.1190/geo2010-0188.1.

Park, C. B., R. D. Miller, and J. Xia, 1999, Multichannel analysis of surface waves: Geophysics, **64**, no. 3, 800–808, https://doi.org/10.1190/1.1444590.

Ritzwoller, M. H., and L. Feng, 2019, Overview of pre-and post-processing of ambient-noise correlations, *in* N. Nakata, L. Gualtieri, and A. Fichtner, eds., Seismic ambient noise: Cambridge University Press, 144–187, https://doi.org/10.1017/9781108264808.007.

Rodríguez Tribaldos, V., J. B. Ajo-Franklin, S. Dou, N. J. Lindsey, C. Ulrich, M. Robertson, B. M. Freifeld, T. Daley, I. Monga, and C. Tracy, 2021, Surface wave imaging using distributed acoustic sensing deployed on dark fiber: Moving beyond high-frequency noise, *in* Y. Li, M. Karrenbach, and J. B. Ajo-Franklin, Distributed acoustic sensing in geophysics: Methods and applications, 197–212, https://doi.org/10.1002/9781119521808.ch15.

Santagata, M., and Y. I. Kang, 2007, Effects of geologic time on the initial stiffness of clays: Engineering Geology, **89**, no. 1-2, 98–111, https://doi.org/10.1016/j.enggeo.2006.09.018.

Schimmel, M., and H. Paulssen, 1997, Noise reduction and detection of weak, coherent signals through phase-weighted stacks: Geophysical Journal International, **130**, no. 2, 497–505, https://doi.org/10.1111/j.1365-246X.1997.tb05664.x.

Schuh, J., 2024, MASW dispersion curve: MATLAB Central File Exchange, https://www.mathworks.com/matlabcentral/fileexchange/65138-masw-dispersion-curve, accessed 25 March 2024.

Shragge, J., J. Yang, N. Issa, M. Roelens, M. Dentith, and S. Schediwy, 2021, Low-frequency ambient distributed acoustic sensing (DAS): Case study from Perth, Australia: Geophysical Journal International, **226**, no. 1, 564–581, https://doi.org/10.1093/gji/ggab111.

Song, Z., X. Zeng, J. Xie, F. Bao, and G. Zhang, 2021, Sensing shallow structure and traffic noise with fiber-optic Internet cables in an urban area: Surveys in Geophysics, **42**, 1401–1423, https://doi.org/10.1007/s10712-021-09678-w.

Spica, Z. J., M. Perton, E. R. Martin, G. C. Beroza, and B. Biondi, 2020, Urban seismic site characterization by fiber-optic seismology:

Journal of Geophysical Research: Solid Earth, **125**, no. 3, https://doi.org/10.1029/2019JB018656.

Stehly, L., M. Campillo, and N. M. Shapiro, 2006, A study of the seismic noise from its long-range correlation properties: Journal of Geophysical Research: Solid Earth, **111**, no. B10, https://doi.org/10.1029/2005JB004237.

Thompson, E. M., B. A. Carkin, L. G. Baise, and R. E. Kayen, 2014, Surface wave site characterization at 27 locations near Boston, Massachusetts, including 2 strong-motion stations: U.S. Geological Survey, open-file report 2014-1232, https://doi.org/10.3133/ofr20141232.

USGS Earthquake Hazards Program, 2024, A risk map of the 50-state NSHM 2023 update showing the greater than MMI6 for chance of damaging shaking within 100 years: USGS Earthquake Hazards Program, https://www.usgs.gov/media/images/a-risk-map-50-state-nshm-2023-update-showing-greater-mmi6-chance-damaging-shaking, accessed 11 October 2024.

White, M. C., Z. Zhang, T. Bai, H. Qiu, H. Chang, and N. Nakata, 2023, HDF5eis: A storage and input/output solution for big multidimensional time series data from environmental sensors: Geophysics, **88**, no. 3, F29–F38, https://doi.org/10.1190/geo2022-0448.1.

Woodhouse, D., P. J. Barosh, E. G. Johnson, C. A. Kaye, H. A. Russell, W. E. Pitt, S. A. Alsup, and K. E. Franz, 1991, Geology of Boston, Massachusetts, United States of America: Environmental and Engineering Geoscience, **28**, no. 4, 375–512, https://doi.org/10.2113/gseegeosci.xxviii.4.375.

Yao, H., and R. D. Van Der Hilst, 2009, Analysis of ambient noise energy distribution and phase velocity bias in ambient noise tomography, with application to SE Tibet: Geophysical Journal International, **179**, no. 2, 1113–1132, https://doi.org/10.1111/j.1365-246X.2009.04329.x.

Yilar, E., L. G. Baise, and J. E. Ebel, 2017, Using H/V measurements to determine depth to bedrock and V_{S30} in Boston, Massachusetts: Engineering Geology, **217**, 12–22, https://doi.org/10.1016/j.enggeo.2016.12.002.

Yu, C., Z. Zhan, N. J. Lindsey, J. B. Ajo-Franklin, and M. Robertson, 2019, The potential of DAS in teleseismic studies: Insights from the Goldstone Experiment: Geophysical Research Letters, **46**, no. 3, 1320–1328, https://doi.org/10.1029/2018GL081195.

Zeng, X., C. Lancelle, C. Thurber, D. Fratta, H. Wang, N. Lord, A. Chalari, and A. Clarke, 2017, Properties of noise cross-correlation functions obtained from a distributed acoustic sensing array at Garner Valley, California: Bulletin of the Seismological Society of America, **107**, no. 2, 603–610, https://doi.org/10.1785/0120160168.